A Device for Mimicking the Contact Force/Contact Area Relationship of Different Materials with Applications to Softness Rendering

Alessandro Serio[1], Matteo Bianchi[1] and Antonio Bicchi[1]

Abstract—In this paper a fabric yielding softness display (FYD–2) is proposed, where the stretching state is controlled using two motors, while the contact area is measured in real-time. In previous works, authors proposed a fabric-based device, with embedded contact area measurement system, which was proved to provide subjects with a compelling and naturalistic softness perception. Compared to it, FYD–2 exhibits reduced dimensions, a more accurate sensorization scheme and an increased actuation velocity, which allows to implement fast changes in the stretching state levels. These changes are mandatory, for example, to properly track typical quadratic force/area curves of real materials. Furthermore, FYD–2 is endowed with an additional degree of freedom that can be used to convey supplementary haptic cues, such as directional cues, which can be exploited to produce more immersive haptic interactions. In this work we describe the mechanical design and the mathematical model of the device. The reliability in real-time tracking of stiffness and force-area curves of real objects is also demonstrated.

I. INTRODUCTION

Softness is the subjective measurement of the compliance of an object. This kind of information is very tactual–related [1] and hence its correct rendering is particularly challenging to guarantee a compelling perception. Regarding the two main modalities of haptic perception, kinaesthesia and tactile information, softness perception basically relies on both, although cutaneous cues play a predominant role in most cases [2].

Different technological solutions have been adopted so far to build suitable haptic devices [3], [4], [5] for softness rendering but the results, although reliable, are still unsatisfactory if compared to the human touch, and the low resolution of stimuli severely affects technical performance. Indeed, the mechanics of touch is very complex, consisting on a huge amount of redundant information processed via many receptors. Therefore, it would be challenging to find suitable *reductions* and approximations of such complexity that can be used to drive the design of artificial systems [6].

Considering cutaneous cues, a possible *reduction* of dynamic, force–varying tactile information operated by nervous system can be represented by the experimentally validated Contact Area Spread Rate (CASR) hypothesis, as it was described in [3]. The CASR paradigm states that, despite the extreme richness of tactile data, *a large part of haptic information necessary to discriminate softness of objects by touch is contained in the law that relates resultant contact force* – being F – *to the overall area of contact* – being A – *or in other terms in the rate by which the contact area spreads over the finger surface as the finger is increasingly pressed*
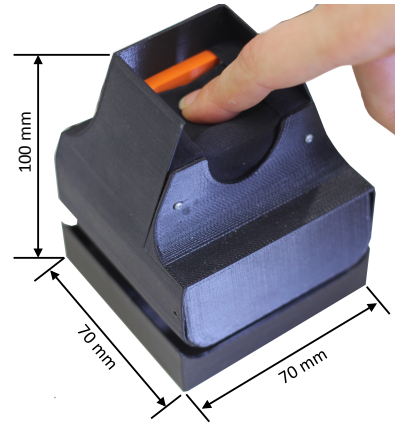

Fig. 1. A subject's finger interacting with FYD–2. The dimensions of the device are also reported.

on the object. Inspired by this force–area relation – being $F(A)$ – it was possible to develop a simple and effective haptic interface such as the pneumatic CASR display presented in [3]. However, although this device was proved to be able to convey a more compelling softness perception if compared to a purely kinaesthetic one, its performance was limited by the lack of real–time contact area measurement, the edge effects due to its "discrete design" (a set of hollow cylinders arranged in a telescopic manner) and the low resolution of the stimuli.

To overcome such limitations, in [7] we proposed a device – the Fabric Yielding Display (FYD) – which exploits the bi–elasticity of a fabric to convey tactual information, providing, at the same time, a measurement in real–time of the contact area of the fingertip/object pair by using a web camera placed just beneath the fabric. This device, because of its naturalistically deformable surface, was proved to be able to enhance softness discrimination accuracy, if compared to the pneumatic one described in [3]. However, although the contact area was actively measured, no contact–area feedback for dynamic tracking was implemented. Here we present a new version of the FYD, hereinafter referred to as FYD–2 (see also fig. 1). The main advantages of this design are: the reduced dimensions, which enable possible integrations with other devices (such as the one proposed in [8]) and wearability; an actuation system based on two fast motors and a more effective sensorization scheme, which consists on a web camera and a force sensor mounted at the base of the device to record the normal contact force exchanged between the finger pad and the fabric. As opposed to the approaches found in literature, where the lack of real–time area measurement severely limits the reliability of tracking $F(A)$ curves by introducing edge effects and

[1]A. Serio, M. Bianchi and A. Bicchi are with the Department of Advanced Robotics, Istituto Italiano di Tecnologia, via Morego, 30, 16163 Genova, Italy and with Centro di Ricerca "E. Piaggio", Università di Pisa, Largo L. Lazzarino, 1, 56100 Pisa, Italy. `{a.serio,m.bianchi,bicchi}` `at centropiaggio.unipi.it`
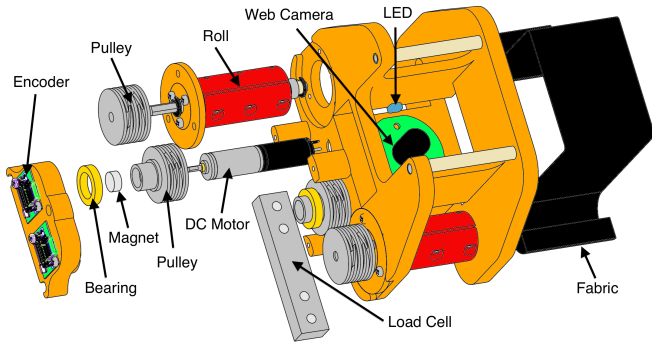
Fig. 2. Exploded draw – in false colors – of the FYD–2. The device main components are reported.

discretization [3] or enabling the control of the fingertip contact area only for a finite set of constructed and stored in advance "numerical models" as in [5], the here proposed actuation and sensorization schemes realize a closed–loop control, which allows to track any arbitrary F(A) characteristic of real specimens. Furthermore, the actuation scheme also endows the system with an additional degree of freedom, which can be used to convey supplementary haptic cues, such as directional information, for a more compelling and immersive haptic experience.

In this work we first describe the mechanical design and characterization of the device. Afterwards we report the description and experimental validation of the mathematical model of the system dynamics. Finally, we discuss the outcomes of the performed experiments, whose aim was to real–time track stiffness values as well as force-area curves of real materials, showing the effectiveness of the here proposed system.

II. MECHANICAL DESCRIPTION

For the realization of FYD–2, we use a layer of isotropic elastic fabric, Superbiflex HN by Mectex S.P.A (Erba, Como, Italy) [7]. Subjects touching the fabric can experience different levels of stiffness, which are obtained by suitably changing the stretching state of the fabric itself.

The extremities of a rectangular strip of the elastic fabric are connected to two rollers, each of them independently moved by a pulley placed on a motor shaft. Motors are DC Maxon Motor REmax (256:1, 3 Watt) by Maxon Motor ag, Sachseln, Switzerland. These motors provide a good trade-off between velocity and torque, thus enabling fast changes in the stretching state of the fabric.

The pulley and the roller are connected by means of a wire transmission. The motor positions are controlled with a custom made electronic board (PSoC-based electronic board with RS–485 communication protocol), which reads motor position by using two absolute magnetic encoders (12 bit magnetic encoder by Austria Microsystems - Unterprem-staetten, Austria - AS5045 with a resolution of 0.0875°).

An exploded drawing of the system is shown in fig. 2. As it is noticeable from fig. 1, the dimensions of the FYD–2 are less than a third of the one exhibited by the previous version of the device [7]. These reduced dimensions can enable the integration with other haptic systems (as proposed, e.g, in [8]) and wearability.

A level of softness is generated by appropriately stretching the fabric using the two motors; ie., when motor 1 rotates in a counter-clockwise direction and motor 2 rotates in a clockwise direction they stretch the fabric thus increasing its apparent stiffness. On the other hand, when motor 1 rotates in a clockwise direction and motor 2 rotates in a counter-clockwise direction they relax the fabric which appears softer (for further details see fig. 3).

It is important to notice that the two motors, when rotating in the same direction, can implement an additional "translational" degree of freedom; i.e. the finger can be moved left and right. Such degree of freedom can be used to convey additional haptic directional information, which can be used to enhance immersiveness of tactual experience. However this aspect is still under investigation.

FYD–2 is also capable to measure the contact area involved in the contact in real-time by placing a web camera (Microsoft "LifeCam HD–3000" with a resolution of 640×480) and two high luminosity LEDs (whose luminosity can be regulated with a trimmer) just beneath the fabric (30 mm), see fig. 2. The segmentation algorithm used to estimate the contact area is based on binarization thresholds heuristically calculated considering the difference between background luminosity and contact area luminosity, as it was described in [7]. An hemispherical cover is placed on the device to guarantee uniform and reproducible luminosity conditions during successive haptic interactions.

Finally, the FYD–2 is endowed with a load cell (Micro Load Cell, 0 to 780g, - CZL616C - from Phidgets, Calgary, Alberta, Canada) placed at the base of the device, to record the normal force exerted by the subject finger interacting with the fabric.

III. CHARACTERIZATION

As it is well known, haptic perception is given by the combination of two different modalities, namely, kinaesthetic perception and cutaneous perception. As in [8], using simplified abstractions and physics concepts, we can consider the $F(\delta)$ curve resulting from the finger touching the object as an approximation of the kinaesthetic information involved in softness perception. F [N] indicates the indenting force and δ [mm] the overall rigid displacement (or indentation) between the two bodies. Analogously, based on the CASR paradigm [3], the $F(A)$ curve can be used to describe the cutaneous cues used for softness discrimination. The stiffness (σ in [N/mm]) of the fabric can be computed directly deriving the contact force w.r.t. the displacement. The $F(\delta)$ characteristics, as they result from the characterization procedure described in the following paragraphs, are quadratic: i.e. $F = \lambda \delta^2$, with λ [N/mm^2] being the quadratic coefficient of the parabolic curve. They were obtained by interpolating the displacement values at fixed motor positions ($R^2 > 0.94$): the stiffness of the uni-axially stretched fabric is hence linear, since it depends on the displacement and it can be defined as (see also [9] and [10])

$$\sigma(\delta) = \frac{\partial F}{\partial \delta} = \rho \delta, \qquad (1)$$

where $\rho = 2\lambda$ [N/mm^2] is the stiffness coefficient.

Notice that, during the characterization of the fabric, the motors were moved at different positions, considering each

time the same angular displacement for both. These angular values, being θ, are within the interval 10° to 80°, with an incremental step of 10°. The stiffness coefficient ρ at $\theta = 10°$ is equal to 0.031 N/mm^2.

A column load frame testing machine (Z005 by Zwick/Roell, Ulm, Germany) was used to compress the fabric, while the indentation and contact force were directly recorded by the machine and the contact area was measured by the web camera placed beneath the fabric. The force/area curves interpolated at fixed motor positions are linear, i.e. $F = \varepsilon A$ ($R^2 > 0.93$). The indenter was moved using fixed indentation steps of 1.5 mm each, for an overall displacement of 12 mm in a time interval of 30 s. The range of the contact force varies from 0 to 20 [N].

We used a wooden hemispherical indenter with a diameter of 14 mm and 100 mm in length, in order to model the last phalanx of a human finger. This diameter was chosen since it is within the typical range of human finger diameter [11]. Differences between the wooden indenter (which is a non–compliant object) and human fingertip (which is a compliant object) should be considered; however, since the deformation of the fingertip interacting with the fabric is small, the approximation of the indenter with a non–deformable object is still acceptable. Indeed, given the range of stiffness that can be reproduced by the device (maximum stiffness 1.4 N/mm, in the range of contact force values from 0 to 20 N), the deformation of the fabric is usually larger than the one produced on the finger pad, given its mechanical properties known from literature [12].

IV. DEVICE MODEL AND VALIDATION

Considering the characterization outcomes, we can model the system with two springs fixed at two pulleys of radius R and inertia $J_1 = J_2 = J$, whose stretching state is related to motor positions (θ_1 and θ_2, respectively, positive for counterclockwise rotations) (cf. fig. 3). Let be K the elastic constant of the springs which model the fabric elasticity, by applying the Lagrangian formulation we get

$$\begin{cases} J_1\ddot{\theta}_1 + c_1\dot{\theta}_1 - K(R\theta_1 - R\theta_2)^2 = \tau_1 + RF\sin\alpha \\ J_2\ddot{\theta}_2 + c_2\dot{\theta}_2 + K(R\theta_1 - R\theta_2)^2 = \tau_2 + RF\sin\alpha \end{cases}, \quad (2)$$

where c_1 and c_2 are the damping coefficients of motor 1 and 2, respectively, τ_1 and τ_2 are the control torques, F is the indentation force exerted by the user and R is the radius of the pulleys.

It is possible to derive also a model–based estimation of the contact area (which we assume to be expressed in [mm^2]). This estimate, if properly validated, might allow us to compute the contact area, without the need to measure it with the web camera. In this manner, we might use this result to drive the design of FYD–2 with further reduced dimensions, in applications where the usage of the camera can be limited for space issues (e.g. device miniaturization for Robot–assisted Minimally Invasive Surgery or integration with complex systems or in multi-finger haptic interfaces). For the model we assume that: the interaction between the finger and the device occurs at the center of the fabric and that the indentation direction is orthogonal to the fabric surface; the finger shape can be modelled with a sphere with a given curvature radius while the contact area is approximated with a circle; the finger deformation is not
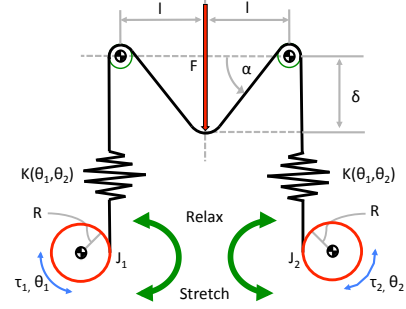

Fig. 3. Schematic representation of the device. The elastic fabric is modeled in a symmetrical fashion with two non linear springs connected to each other by means of an inextensible wire. The model springs are thought to be fixed at two pulleys of radius R and inertia $J_1 = J_2 = J$, and they stretching state changes according to motor positions (θ_1 and θ_2). When the fingertip interacts with the fabric exerting a vertical force (F), the length of the springs as well as the geometry of the fabric are changed.
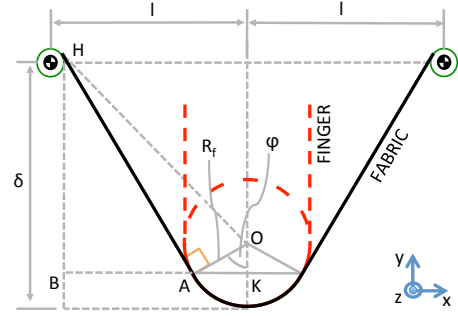

Fig. 4. Sketch of the fingertip (red dashed line circle) contacting the elastic fabric (black line). φ is the angle between the normal passing through O – the center of the sphere (with radius R_f) modelling the fingertip – and the segment connecting O and A, i.e. the point on the fabric tangent to the sphere. δ is the indentation that the fingertip produces on the fabric, while l is the half length of the fabric tactile surface. The z axis is oriented out from the xy plane.

relevant w.r.t. the deformation of the fabric; the elasticity of the fabric can be modeled in a symmetrical fashion, by means of two non linear springs connected to each other by an inextensible wire.

After force exertion, the fabric geometry will change. The parameter α defines the angle between the fabric surface at rest and the indented surface. To compute α parameter is hence mandatory to get the indentation δ. To do it, it is possible to exploit motor position known from motor encoders to obtain θ and hence λ value, i.e. the coefficient of the $F(\delta)$ quadratic curve, as it results from the characterization curves or interpolating between them. Notice that in our case we have $\theta_1 = -\theta_2 = \theta$. By knowing the actual contact force F measured by the load cell placed at the base of the device, δ value is computed as

$$\delta = \sqrt{F/\lambda} \quad (3)$$

and hence $\alpha = \arctan(\delta/l)$, where l is the half length of the fabric tactile surface. For further details see figs. 4 and 3.

The model contact area (A_{mo}) will be
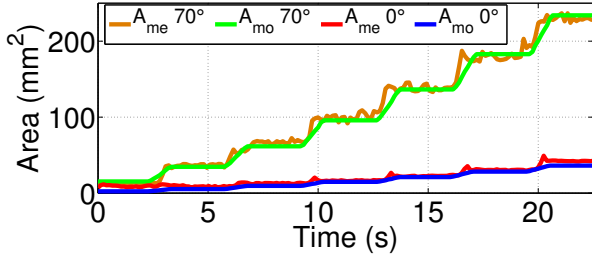
$$A_{mo} \approx \pi(R_f \sin\varphi)^2, \quad (4)$$

Fig. 5. Results of model validation at three different motor positions. A_{mo} is the contact area estimated with the model while A_{me} is the measured one.

θ ($°$)	RMSE (mm^2)	PRMSE ($\%$)	C. F.	CRMSE (mm^2)	PCRMSE ($\%$)
0	102	49	1.94	8.7	2.1
10	63.1	30.1	1.56	11.9	3.6
20	34.5	18.3	1.36	10.1	3.9
30	22.6	18.2	1.30	10.8	5.6
40	15.8	12.8	1.24	8.0	5.2
50	8.7	53.2	0.86	3.4	3.3
60	10.7	12.1	0.8	3.2	4.5
70	45.4	33.7	0.3	4.4	9.9

where $R_f = 7\ mm$ [11] is the curvature radius of the fingertip (i.e. the radius of the sphere) and it is a free parameter of the model. φ is the angle between the normal passing through O – the center of the sphere modelling the fingertip – and the segment connecting O and A, the latter is the point on the fabric tangent to the sphere modelling the fingertip.

A_{mo} is centered at the point K and it is parallel to the xz plane and orthogonal to the xy plane, passing trough point A. Knowing the indentation of the fabric produced by the fingertip (δ) from equation (3), we can define the indentation of the sphere center as

$$\bar{\delta} = \delta - R_f, \qquad (5)$$

δ (and $\bar{\delta}$) is time dependent since it is strictly linked to the indentation force. For sake of readability, in the following, time dependency of δ is omitted. Computing segments $\overline{HO}$, $\overline{HA}$ and $\overline{HB}$ as

$$\overline{HO} = \sqrt{l^2 + \bar{\delta}^2},$$

$$\overline{HA} = \sqrt{\overline{HO}^2 - R_f{}^2} = \sqrt{l^2 + \bar{\delta}^2 - R_f{}^2}, \qquad (6)$$

$$\overline{HB} = \bar{\delta} + R_f \cos\varphi,$$

and considering that

$$\sin\varphi = \overline{HB}/\overline{HA}, \qquad (7)$$

angle φ can be obtained using tangent parametric formulation as

$$\varphi_{1,2} = 2\arctan\left(\frac{\overline{HA} \pm l}{\bar{\delta} - R_f}\right). \qquad (8)$$

and hence A_{mo} can be calculated.

A. Model Validation

In order to validate the proposed model, we have compared the contact area measured by the web camera (A_{me}) with the contact area computed by the model (A_{mo}) obtained during the characterization procedure. Root Mean Square Errors (RMSEs) between A_{mo} and A_{me}, over all the force-area characterization curves, are considered.

Without affecting the goodness-of-fit of the model, we introduce a correcting scaling factor (different for each characterization curve), hereinafter referred to also as C.F. (see the fourth column of table I). The correction factor (C.F.) is defined as the scaling factor between the measured area and the model - based area, and it is computed from the experimental data. In order to assess the effectiveness of the here proposed contact area model, it is important to know how much predictable the correction factor is. To achieve this goal we have performed a regression between the correction factor values and the corresponding motor positions. Using the following linear function

$$CF(\theta) = 0.02\theta + 0.46, \qquad (9)$$

we have a goodness of fit of $R^2 = 0.94$.

We have computed RMSE (the second column of table I) values also in this case, referring to it as CMRSE, with the letter C standing for Correction (cf. the fifth column of table I).

In fig. 5 we report the comparison results for three motor positions, while in table I we report the root mean square errors of the comparison for each characterization curve with and without the correction factor. For sake of completeness we also report the percentage RMSE normalized by the maximum value of contact area measured at a a given position of the motor. We refer to it as a RMSE Percentage (RMSEP, the third column of table I). The same approach is applied to CRMSE, leading to Percentage CRMSE or CRMSEP (cf. the sixth column of table I).

What is noticeable is that the model is able to estimate the contact area with a good level of accuracy: considering the correction factor the maximum percentage of error is less than 10%.

V. EXPERIMENTS

Since softness perception relies on both haptic channels – kinaesthesia and cutaneous information –, FYD–2 can be controlled to track $F(\delta)$ or $F(A)$ curves. Of course both characteristics are strictly related each other in the device (for a decoupling strategy of these characteristics, see e.g. [8]).

When the system behaves like a $F(\delta)$ tracker, i.e. to mimic a given stiffness, the behavior is analogous to the one exhibited by common kinaesthetic systems (which basically act as force displays [13]), although cutaneous cues are clearly conveyed to subjects via fabric deformation. Furthermore, the measurement of the contact area in real–time is now available and it can provide additional tactile information about the haptic interaction in act.

(a) Stiffness Control
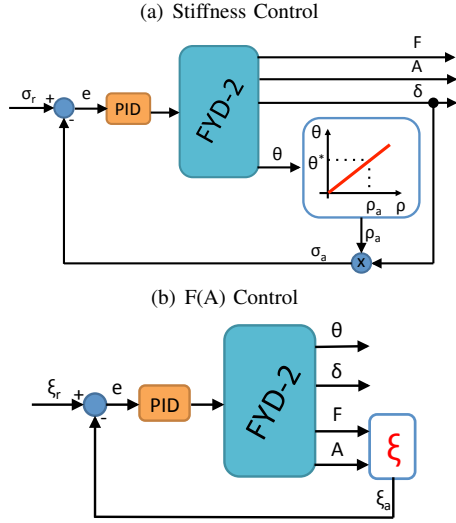
(b) F(A) Control

Fig. 6. In the plot (a) we report the block diagram of the control used for constant stiffness tracking experiments, while in the plot (b) the block diagram of the control applied for F(A) tracking is shown.
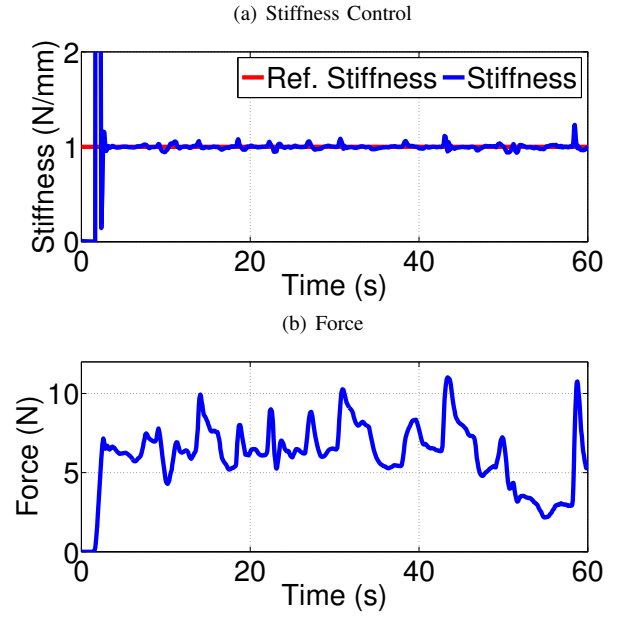

(a) Stiffness Control

(b) Force

Fig. 7. In (a): stiffness control (blue line) vs. stiffness reference (red line). In (b): the measured force is reported.
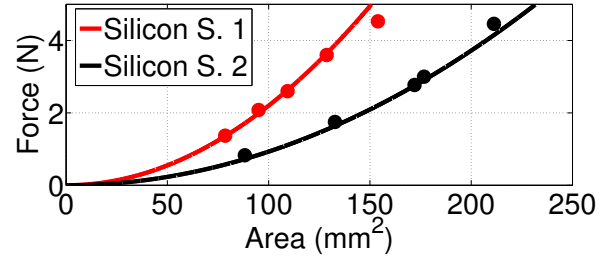

Fig. 8. Experimental $F(A)$ characteristics of two silicon specimens.

A. Constant Stiffness Tracking

The aim of the experiments here reported is to track a constant stiffness, being σ_r. The indenter was the finger pad of a male subject (age 32) probing the fabric, with a frequency of approximately 1 Hz. Since the fabric stiffness is not constant but it depends on the indentation, we need to suitably control motor positions using motor encoders to know θ value. From this value it is then possible to retrieve the angular coefficient (ρ_a in [N/mm^2]) of the actual stiffness curve, from the characterization characteristics or interpolating between them. Using the information about the contact force measured by the load cell of the device, the actual indentation δ can be obtained as in equation (3). Finally, the actual stiffness (σ_a in [N/mm]) of the fabric can be computed as $\sigma_a = \rho_a \delta$.

In this experiment, the purpose was to track a constant stiffness $\sigma_r = 1\,N/mm$. We use PI control to move the motor positions to θ_r, based on the error (e) between σ_r (reference stiffness) and σ_a (actual stiffness), with heuristically found constants $P = 1$, $I = 0.01$.

In fig. 7 the results of the control are reported. In this case, after an initial transitory phase due to motor positioning, we get an RMSE of 0.1879 N/mm, less than 20% w.r.t. the reference value. The effect of this phase on human perception will be investigated in future psychophysical experiments.

B. Trajectory Area Tracking

The $F(A)$ characteristics obtained during the characterization phase are linear at fixed motor positions; therefore, linear $F(A)$ curves can be simply mimicked by using or interpolating across motor positions the characterization plots. However, in order to reproduce common quadratic $F(A)$ characteristics [3], the position of the motors needs to be controlled and suitably rapidly changed, based on the actual contact area. This fact motivated the need for a fast actuation system. Let be $F(A) = \xi_r A_r^2$, the quadratic curve to be tracked, with ξ_r in [N/mm^4] is the quadratic coefficient of

the area. In order to properly implement the control, we need to know the actual ξ_a [N/mm^4] coefficient. This coefficient is obtained each time by dividing the indenting force measured by the load cell for the squared value of the measured area A_m or the model–based area A_{mo}. Indeed, force/area tracking performance are evaluated using both the measured area and the model–based estimation of the contact area.

PI control is then used to move the motors, based on the error between the reference coefficient ξ_r and the actual one ξ_a (see fig. 6(b)).

In this case, the PI constants are heuristically set as: $P = 5$ and $I = 0.3$.

To properly validate the system performance in $F(A)$ tracking, two different silicon specimens, specimen 1 and specimen 2, were chosen to be reproduced. We derived the properties between the contact force and the contact area, by measuring the indented force while the silicon specimen was indented by the fingertip. The specimen was placed on a load-cell and the surface of the material covered by a transparent plastic sheet. The finger pad was colored using ink. The contact area was obtained by measuring the scanned contact area images, at fixed values of contact force. For each level of force, a scanned image was associated. The
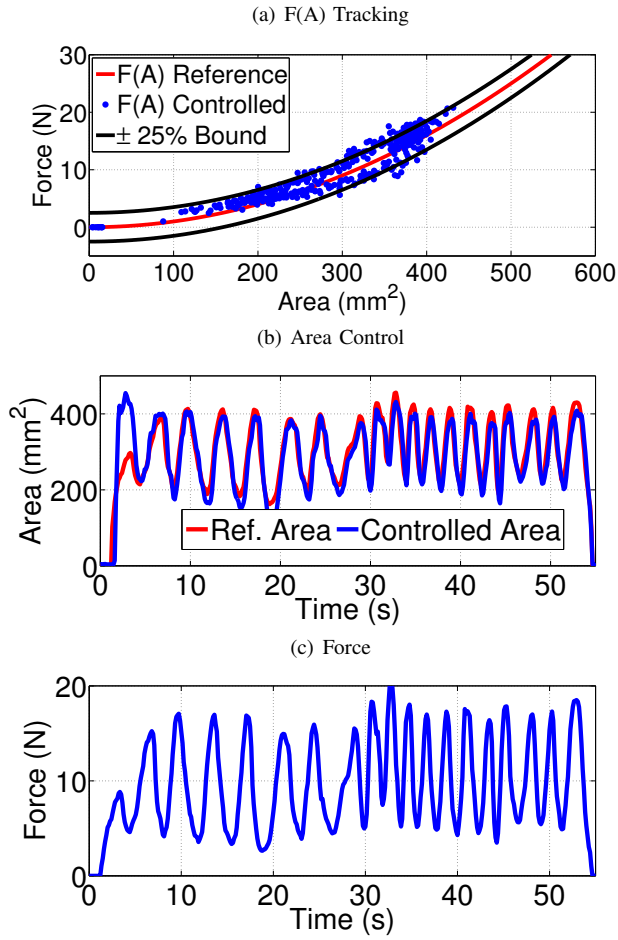
(a) F(A) Tracking

(b) Area Control

(c) Force

Fig. 9. In the first plot (a) we show the reference $F(A)$ curve (in red), while the pairs (measured controlled area, measured force) are represented as blue dots. The $\pm 25\%$ interval bounds w.r.t the reference curve are represented as black lines. In the second plot (b) we report the contact area control (blue line) vs. contact area reference (red line). In the third plot (c) the measured force is reported. These plots refer to the silicon specimen 1.
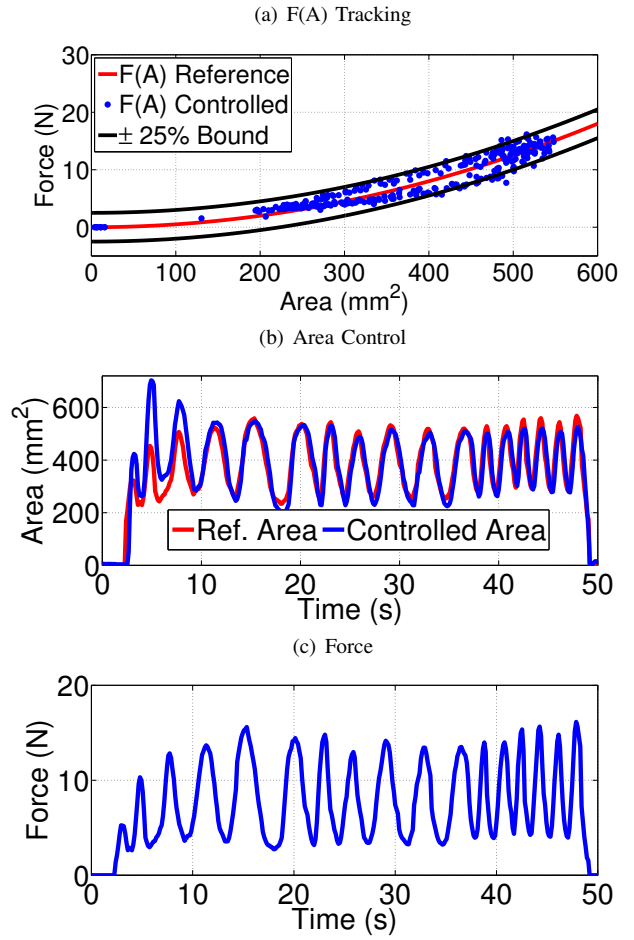

(a) F(A) Tracking

(b) Area Control

(c) Force

Fig. 10. In the first plot (a) we show the reference $F(A)$ curve (in red), while the pairs (measured controlled area, measured force) are represented as blue dots. The $\pm 25\%$ interval bounds w.r.t the reference curve are represented as black lines. In the second plot (b) we report the contact area control (blue line) vs. contact area reference (red line). In the third plot (c) the measured force is reported. These plots refer to the silicon specimen 1.

couples[1] contact area/contact force were then interpolated using a quadratic function, which lead to ξ coefficients of 0.83×10^{-4} and 1.4×10^{-4} [N/mm^4] for the specimen 1 and specimen 2, respectively ($R^2 > 0.91$).

The procedure is analogous to the one reported in [5]. The characteristics are reported in fig. 8. The contact force was within the range of 0.5 to 4.5 N.

The $F(A)$ tracking experiments were performed by a male subject (age 32) touching the fabric with his index finger pad, using a probing frequency of approximately 1 Hz.

The $F(A)$ tracking results are reported in fig. 9 and fig. 10 for the silicon specimens 1 and 2, respectively. In these cases, the couples (Measured Controlled Area, Measured Force) are indicated as blue dots.

For specimen 1, $\sim 92.5\%$ of the controlled couples is within the $\pm 25\%$ of the reference bounds, while for specimen 2, $\sim 94.3\%$ of the controlled couples is within the $\pm 25\%$ of the reference bounds. This value for the reference bounds is chosen since it is common in statistics, expressing the

[1]the term *couple* indicates the Contact Area and the corresponding Contact Force that represent the coordinates of a point in the $F(A)$ plane

quartile of a distribution. A possible explanation for the observable bias in $F(A)$ tracking might be related to the hysteresis of the fabric.

The corresponding reference area is tracked with a RMSE of 37.7 mm^2 and a RMSEP of 9.8% (w.r.t. the reference value), for the specimen 1 (cf. fig. 8), and for specimen 2 we get a RMSE of 34.3 mm^2 and a RMSEP of 11.2%.

We have also performed a $F(A)$ tracking experiments using as feedback signal the model-based area, using correction factors, as it is shown in fig. 11. For sake of space we only report results about the tracking performance for specimen 1.

With the model-based area, the corresponding reference area is tracked with a RMSE of 80.2 mm^2 and a RMSEP of 17.8% , while $\sim 64.7\%$ of the controlled couples is within the $\pm 25\%$ of the reference bounds.

Results are encouraging, suggesting that model–based control can provide satisfactory outcomes –although, of course, inferior to the ones achievable with the actual measurements of the area – thus representing a good trade–off control scheme in applications where the usage of the camera can

(a) F(A) Tracking
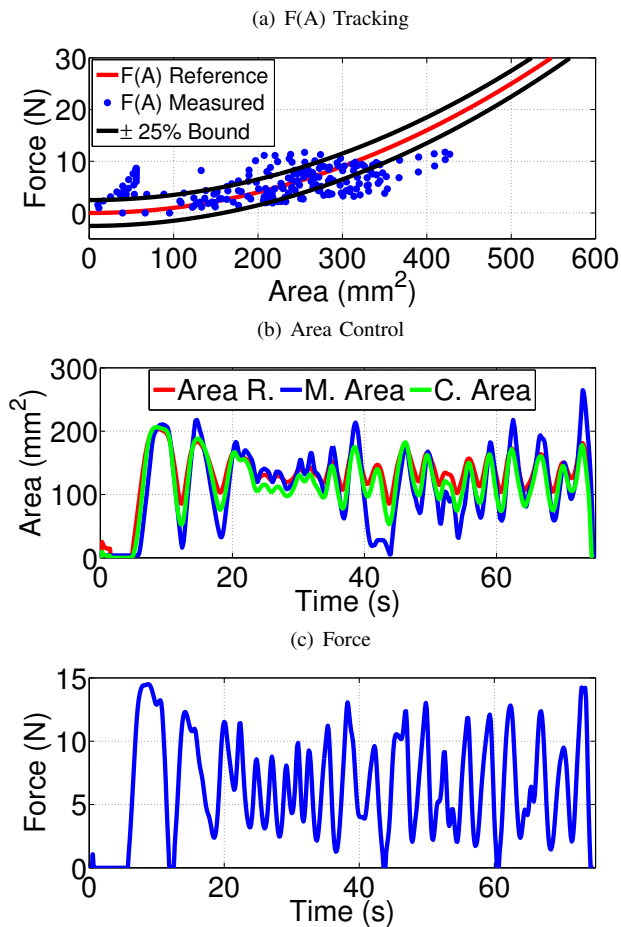

(b) Area Control

(c) Force

Fig. 11. In the first plot (a) we show the reference $F(A)$ curve (in red), while the pairs (measured controlled area, measured force) are represented as blue dots. The $\pm 25\%$ interval bounds w.r.t the reference curve are represented as black lines. In the second plot (b) we report the controlled contact area (green line), as it results from the model, contact area reference (red line) and the actual measured contact area (blue line). In the third plot (c) the measured force is reported. These plots refer to the silicon specimen 1.

be limited, e.g. for space issues (device miniaturization).

However, the most important result is that, to the best of our knowledge, for the first time, force-area curves can be reproduced using our system on the basis of feedback of real-time measured area.

VI. CONCLUSIONS AND FUTURE WORK

In this work, we present a fabric yielding softness display (FYD–2), which is able to mimic different softness information suitably controlling the fabric stretching state, while the contact area is measured in real-time. A model of the device behavior which allows to estimate the contact area is also provided and validated; apart from scaling factors, the model furnishes good results and this fact might be used to drive the design of FYD–2 system and achieve a possible further reduction in its dimensions. The system has been proved to be able to mimic any given constant stiffness value and – much more important – it has been proved to be able to provide a reasonably accurate tracking of $F(A)$ curves, by using for the feedback both the information of contact area measured in real-time and the model–based estimated area.

Also in this latter case, results are encouraging, although inferior to the ones achievable by directly measuring the contact area.

Additionally, since FYD–2 is endowed with two motors that can coherently rotate, there is an additional degree of freedom that can be used to convey supplementary haptic cues, such as directional information.

Future works will focus on investigating the possibilities to properly use this additional degree of freedom; psychophysical experiments to validate the here proposed $F(A)$ tracking are also planned. Integration with vibrational feedback represents another challenging issue.

ACKNOWLEDGMENT

REFERENCES

[1] S. L. Lederman and R. L. Klatzky, "Relative availability of surface and object properties during early haptic processing," *Journal of Experimental Psychology: Human Perception and Performance*, vol. 23, no. 6, pp. 1680–1707, December 1997.

[2] M. A. Srinivasan and R. H. LaMotte, "Tactile discrimination of softness," *Journal of Neurophysiology*, vol. 73, no. 1, pp. 88–101, June 1995.

[3] A. Bicchi, D. E. De Rossi, and E. P. Scilingo, "The role of the contact area spread rate in haptic discrimination of softness," *IEEE trans. on Robotics and Automation*, vol. 16, no. 5, pp. 496–504, October 2000.

[4] V. H. V. Levesque, J. Pasquero and M. Legault, "Display of virtual braille dots by lateral skin deformation: Feasibility study," *ACM Trans. on Applied Perception*, vol. 2, no. 2, pp. 132–149, April 2005.

[5] K. Fujita and H. Ohmori, "A new softness display interface by dynamic fingertip contact area control," in *World Multiconf. on Systemics, Cybernetics and Informatics*, Orlando, Florida (USA), July 2001, pp. 78–82.

[6] M. Bianchi, "On the role of haptic synergies in modelling the sense of touch and in designing articial haptic systems," Ph.D. dissertation, 2012.

[7] M. Bianchi, A. Serio, E. P. Scilingo, and A. Bicchi, "A new fabric-based softness display," in *Proc. IEEE Haptics Symposium*, 2010, pp. 105 –112.

[8] E. P. Scilingo, M. Bianchi, G. Grioli, and A. Bicchi, "Rendering softness: Integration of kinaesthetic and cutaneous information in a haptic device," *IEEE Transactions on Haptics*, vol. 3, no. 2, pp. 109 – 118, 2010.

[9] G. Grioli and A. Bicchi, "A real-time parametric stiffness observer for vsa devices," in *2011 IEEE International Conference on Robotics and Automation*, Shanghai, China, May 2011.

[10] A. Serio, G. Grioli, I. Sardellitti, N. Tsagarakis, and A. Bicchi, "A decoupled impedance observer for a variable stiffness robot," in *IEEE International Conference on Robotics and Automation*, Shanghai, China, May 2011.

[11] "3-d finite-element models of human and monkey fingertips to investigate the mechanics of tactile sense," *ASME, J. of Biomech. Eng.*, vol. 125, pp. 682–691, 2003.

[12] G. J. Gerling, "Sa-i mechanoreceptor position in fingertip skin may impact sensitivity to edge stimuli," *Applied Bionics and Biomechanics*, vol. 7, no. 1, pp. 19 – 29, 2010.

[13] B. Hannaford and A. M. Okamura, *Springer Handbook on Robotics*. Heidelberg, Germany: Springer, 2008, ch. Haptics, pp. 719–739.